

Supplementary Material

Capillary ionic liquid electrospray: beam compositional analysis by orthogonal time-of-flight mass spectrometry

S. W. Miller¹, J. R. Ulibarri-Sanchez^{2‡}, B. D. Prince^{3†} and R. J. Bemish³

¹Boston College, Institute for Scientific Research, Chestnut Hill, MA 02467, USA

²Universities Space Research Association, Houston, TX 77058, USA

³U.S. Air Force Research Laboratory, Space Vehicles Directorate, Kirtland AFB, NM 87117, USA

Supplemental

This supplemental section provides additional material that may aid the reader in evaluating the results of this study.

S.1. Additional Spectra and Derived Results

In addition to BMI-DCA data, mass spectra were taken for EMI-IM, BMI-IM, and BMI-BF₄. These mass spectra were collected over the nominal potential values of ± 300 V to ± 900 V at discrete volumetric flow rates of 0.28 to 1.99 nL/s, 0.63 to 2.97 nL/s, and 1.0 to 1.38 nL/s for EMI-IM, BMI-IM, and BMI-BF₄, respectively. Representative mass spectra, the sum of the various collected kinetic energy spectra, obtained using the orthogonal TOF instrument are shown in figure S1 for EMI-IM, BMI-IM, and BMI-BF₄. Depending on the ILs, the abscissa axis spans out to 800,000 amu/q and plotted against a linear ordinate axis. The trends illustrate the impact of using different ΔE values when iterating the base DC potential on the pulsing region plates from ± 300 V to ± 900 V. EMI-IM data was collected using a ΔE value of 100 eV/q. This resulted in increased uncertainty in the data trends. BMI-IM data was collected using a ΔE value of 25 eV/q and resulted in the least uncertainty in the data trends. BMI-BF₄ data was collected at an intermediate value of 50 eV/q. In each of the three figures of figure S1, both the *low m/q* and *high m/q* droplet distributions are shown. The trends at the lowest flow rates of the three ILs illustrate the most apparent *low m/q* droplet distribution and with increasing flow rate the *low m/q* droplet either reduces in intensity or disappears from the spectrum. The *high m/q* droplet components are the distributions of interest in figure S1. At the lowest flow rate for each IL, the *high m/q* droplet *m/q* breadth is narrow. For BMI-IM the *high m/q* droplet extends out to 500,000 amu/q while EMI-IM and BMI-BF₄ extends out to no more than 350,000 amu/q. At each subsequent increase in flow rate in each IL, the breadth of the *high m/q* droplet distribution expands to higher *m/q* values. At the highest flow rate, BMI-IM *high m/q* distribution extends out to 800,000 amu/q while EMI-IM and BMI-BF₄ distributions extend out to at most 600,000 amu/q. The overall maximum intensity, which coincides at the centroid value of the distributions, of the *high m/q* droplet distribution in each IL occurs at the lowest flow rate. For each subsequent increase in flow rate in each IL, the intensity at the centroid of the *high m/q* droplet distribution is reduced compared to the previous flow rate. The extension and height reduction of the *high m/q* droplet occur simultaneously with

[†] Email address for correspondence: afrl.rvborgmailbox@us.af.mil

[‡] Currently: Systems Engineer, Northrop Grumman

increasing flow rate and suggests that the m/q of the electro spray beam is broadened over more m/q channels, but with a population reduction in each m/q channel.

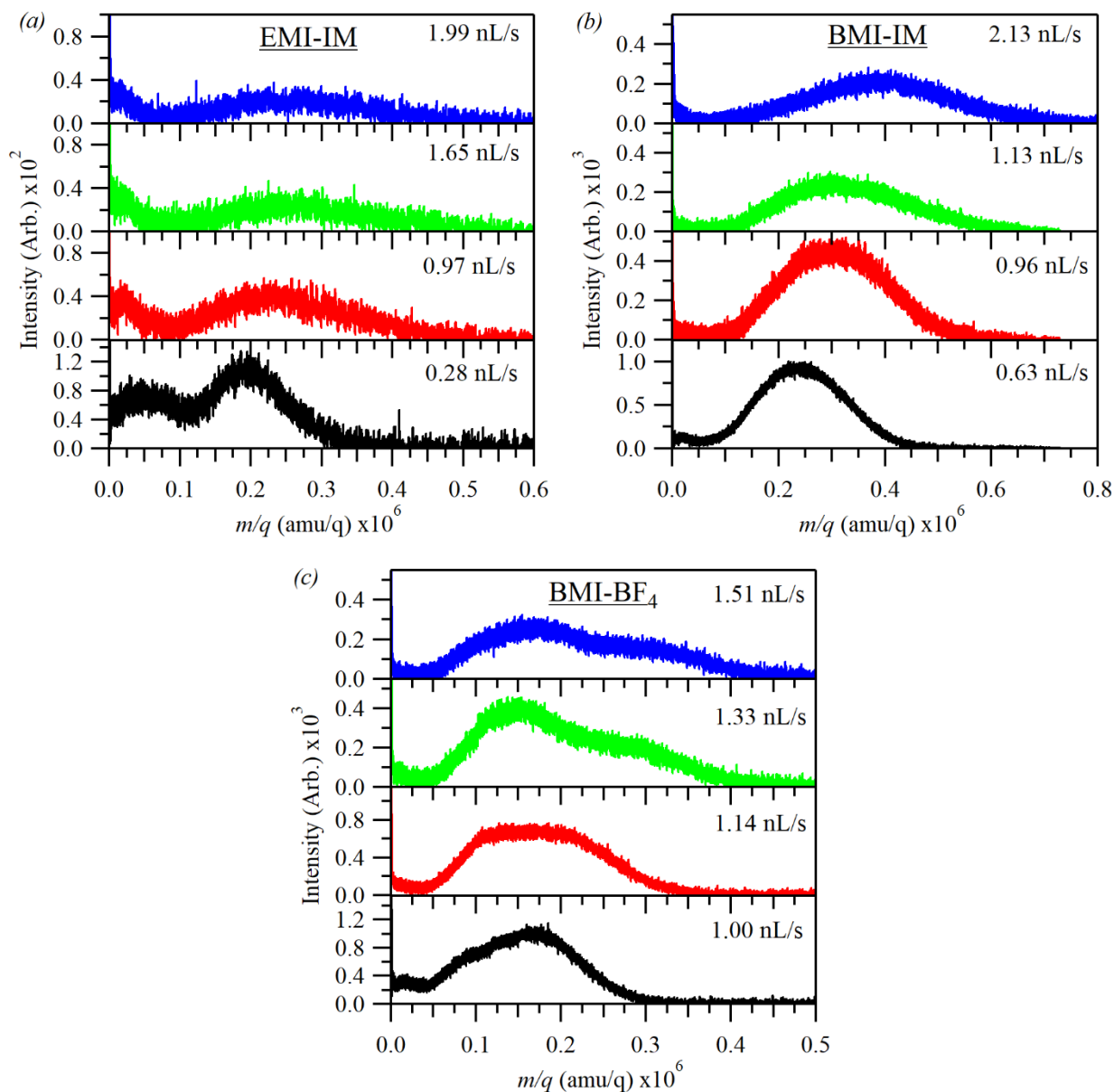


FIGURE S1. Mass spectrum for four flow rates of ILs: (a) EMI-IM; (b) BMI-IM; and (c) BMI-BF₄. The data illustrates the *high* m/q droplet component of the mass spectrum out to 800,000 amu/q. Each flow rate spectrum is a composite of the per ΔE spectrum for each IL. ΔE values used for each IL are: EMI-IM – 100 eV/q, BMI-IM – 25 eV/q, and BMI-BF₄ – 50 eV/q.

An example of the typical energy defect dependence in the anion polarity for the two log-normal distributions is shown in figure S2 for BMI-IM at 0.96 nL/s. In this deconstructed form, the individual mass spectrum per ΔE provide specific information regarding the kinetic energy properties of the two droplet distributions. The mass spectra for BMI-IM were obtained at a ΔE interval of 25 eV/q. Figure S2(a) illustrates the five select unprocessed mass spectra for BMI-IM

at ΔE values of 100, 200, 300, 400, and 500 eV/q. The *low m/q* droplet distribution is only intense at high ΔE values. At lower ΔE values the *low m/q* droplet distribution is either much less intense or not present when compared to the *high m/q* droplet distribution. The *high m/q* droplet distribution is apparent at 400 eV/q with an associated centroid m/q value at approximately 100,000 amu/q. For every 100 eV/q decrease in ΔE , the centroid m/q value shifts further along the abscissa axis to approximate values of 200,000, 325,000, and 400,000 eV/q. As expected, an expansion of the *high m/q* droplet distribution simultaneously occurs with the shifting centroid as well as a reduction in intensity at the associated centroid of the distributions. Noticeably, the higher m/q values are associated with lower ΔE values or higher kinetic energies. Figure S2(b) shows the fitted spectrum results of the *low* and *high m/q* droplets at increments of 25 eV/q for BMI-IM. The bottom panel shows the *low m/q* droplet component and the top panel shows the *high m/q* droplet component. The fits illustrate that the *low m/q* droplets are not present in the electrospray beam until the energy defect reaches 350 eV/q. As ΔE is increased, the *low m/q* droplet becomes a greater component of the beam and reaches maximum intensity at 500 eV/q. After that energy defect value, the *low m/q* droplet contribution in the beam begins to decrease to almost the same as that of the 350 eV/q. During the evolution of the *low m/q* droplet into the beam, the centroid of the droplet remains fixed and the breadth of the distribution mostly remains within 150,000 amu/q. For the *high m/q* droplet, the droplet contributes to the electrospray beam at the lowest ΔE scanned of 100 eV/q. The *high m/q* distribution progresses across the m/q axis. At 100 eV/q, the centroid of *high m/q* distribution is centered on 375,000 amu/q. With increasing ΔE , the centroid shifts to lower m/q values and is centered over 50,000 amu/q by 500 eV/q. Over the increase in ΔE , the maximum intensity at the centroid increases in value and the distribution breadth narrows. After 500 eV/q, the *high m/q* droplet distribution begins to decrease and merges into the *low m/q* distribution.

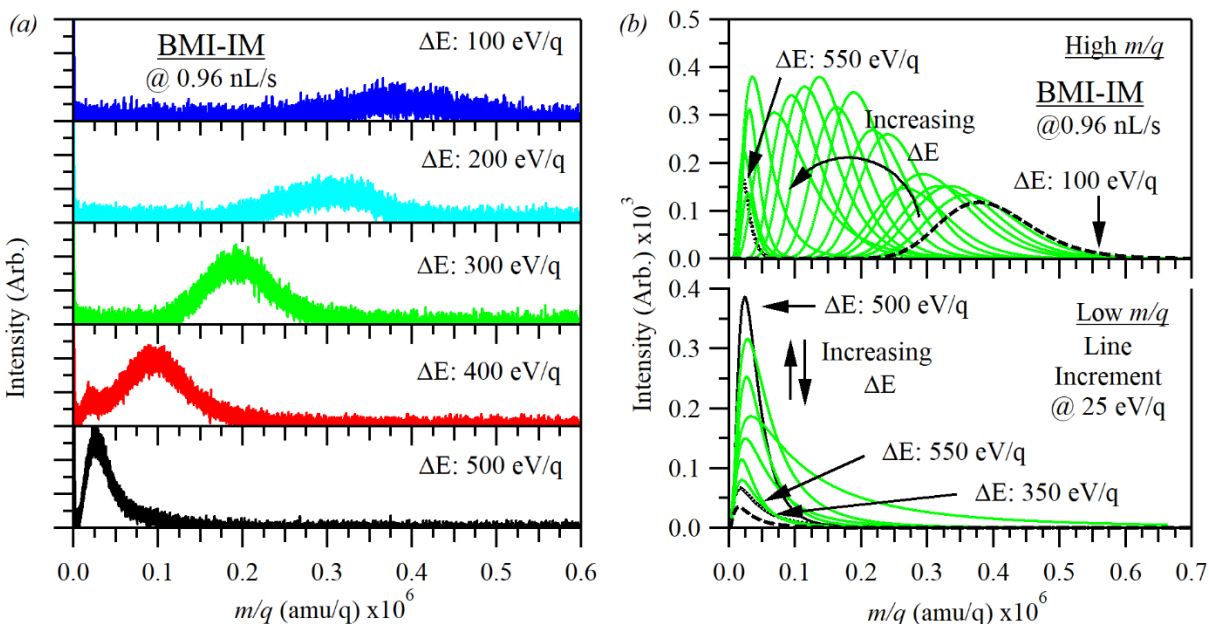


FIGURE S2. Mass spectrum of anion emission of BMI-IM at 0.96 nL/s. (a) Raw data at ΔE increments of 100 eV/q showing the evolution of just the *low m/q* droplet (ΔE : 500 eV/q), formation of the *high m/q* droplet (ΔE : 400 eV/q),

and the loss of the low m/q droplet (ΔE : 300+ eV/q). The two droplets coexist at higher ΔE values. (b) Fitted spectrum results of the low and high m/q droplets at increments of 25 eV/q. The lower plot is of the low m/q droplet component and the upper plot is of the high m/q droplet component. Lowest ΔE value – long dash fit, highest ΔE value – small dash fit.

Figure S3 illustrates a highly resolved anion mass spectrum at the specific ΔE value of 550 eV/q. In figure S3, the spectrum is generated by summing four million sweeps resulting in highly resolved charged species under 40,000 amu/q. The bottom panel is the full spectrum out to 40,000 amu/q highlighting the ion region on the left and the low m/q droplet on the right. The cyclical pattern to the ions illustrates the appearance of doubly-charged, triply-charged, and multiply-charged ions. The top panel of figure S3 is magnified on the region under 10,000 amu/q. At this magnification, the periodic pattern becomes clearer and more structured. Above 5,000 amu/q, the ion peaks become an oscillation on the rising low m/q droplet distribution. From this highly resolved spectrum, we can conclude that the log-normal distribution of the low m/q is in fact the result of the system inability to fully resolve all the charged species present in the beam at this m/q range. When charged species become higher-order charged and increase in mass, the variety of populated m/q configurations result in overlapping m/q values forming a distribution.

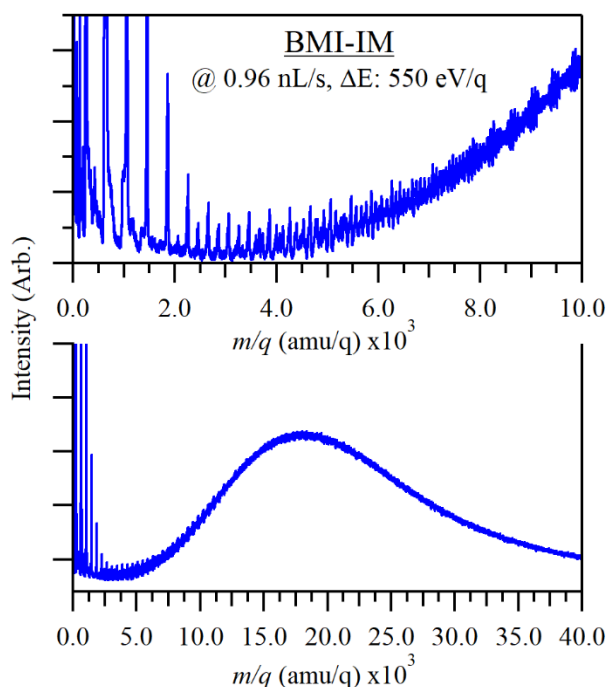


FIGURE S3. Mass spectrum of anion emission of BMI-IM at 0.96 nL/s for 550 eV/q. Bottom figure shows the low m/q ion region and the low m/q droplet region out to 40,000 amu/q. Top figure magnifies the region from 0 to 10,000 amu/q to highlight the diverse set of emitted m/q species detected.

The *high* m/q droplet centroid data plotted as DC potential vs. $\frac{1}{2} m/q$ (all in SI units) is presented in figure S4 for the ILs BMI-DCA, EMI-IM, and BMI-BF₄ at several selected flow rates. Since data for BMI-DCA and EMI-IM were collected at an ΔE interval of 100 eV/q (see figure S4(b,c)), only a few centroid data points are used for each flow rate. Due to this, the linear data fits are more uncertain than the fits of BMI-BF₄ where that data was collected at an ΔE interval of

50 eV/q or the fits of EMI-IM at an ΔE interval of 25 eV/q. The square root of the slope of the fits correspond to the jet velocity. The ordinate intercept of the fits corresponds to the potential at the jet tip or moment of droplet separation. As indicated by the open symbols, the ions have a corresponding potential with the tip potential at each of the flow rates.

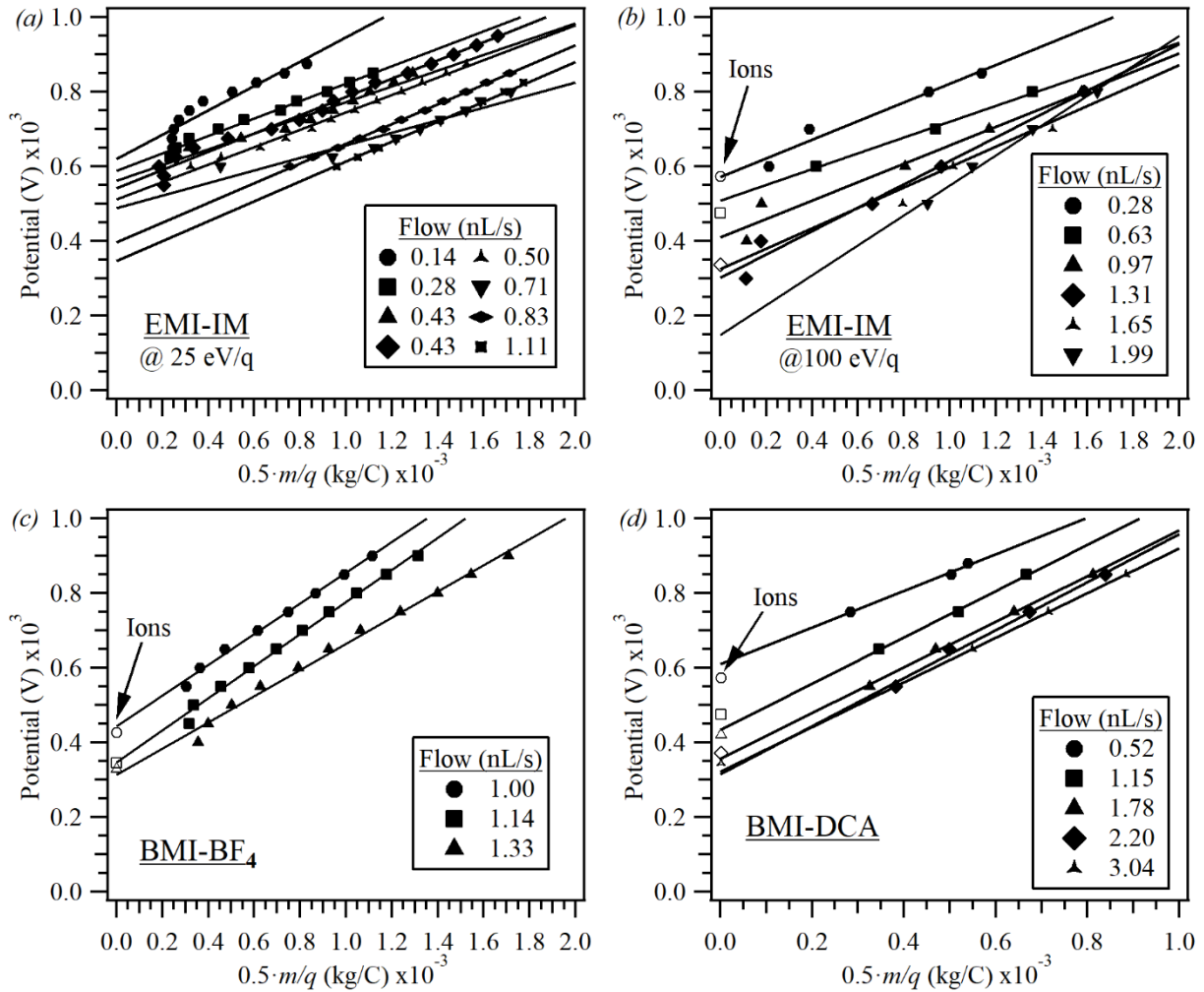


FIGURE S4. Plots of potential versus mass-to-charge ratio for (a), EMI-IM at a 25 eV/q interval (b) EMI-IM at a 100 eV/q interval, (c) BMI-BF₄, and (d) BMI-DCA. The data points represent the high m/q droplet distribution centroids for select flow rates. Note the open symbols represent the singly-charged ions $n = 0 - 5$ at each flow rate and correspond to the y-intercept potentials, Φ_{Tip} .

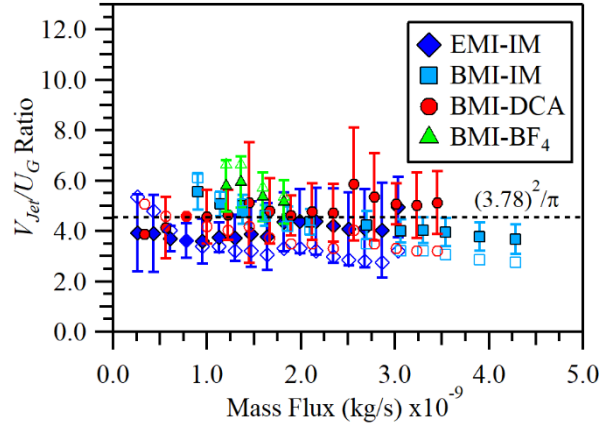


Figure S5. Comparison of the V_{Jet}/U_G (filled markers) and v_0/U_G (open markers) values, where v_0/U_G simply equals $[2 \cdot (R_{Drop}/R_{Jet})]^2/\pi$. U_G is the characteristic velocity from Gañán-Calvo and Montanero (2009).

It was noted in discussing figure 10(b) that the characteristic velocity, v_0 , of each IL is of the same order as the jet velocity extracted from the collected data and falls within the jet velocity uncertainties. v_0 presented in figure 10(b) are U_G (Gañán-Calvo & Montanero 2009) scaled by a factor associated with the radius ratio of 1.89 and can be expressed as $v_0/U_G = [2 \cdot (R_{Drop}/R_{Jet})]^2/\pi$. Unfortunately, the v_0 lines can deviate from velocity values at discrete flow rates. v_0 can be tailored to each flow rate by equating the radius ratio R_{Drop}/R_{Jet} to R_D/R_{Jet} as determined from the linear stability analysis and listed in table 4. Figure S5 illustrates both v_{Jet} and the tailored v_0 normalized by U_G . The values of the two ratios are scattered about the line of $3.78^2/\pi$, which represents a radius ratio of 1.89. v_{Jet}/U_G values are represented by the filled markers, while v_0/U_G are presented by the corresponding open markers. Unlike using 1.89, each unique R_D/R_{Jet} value results in a scaling that places v_0/U_G with the uncertainty of v_{Jet}/U_G . Using the specific R_D/R_{Jet} value at each flow rate provides a better approximation of v_0 to the V_{Jet} value. There appears to be correspondence between Gañán-Calvo's characteristic velocity and the jet velocity determined from experimentation via the R_D/R_{Jet} at each flow rate.

S.2. Additional Information from Droplet Breakup Simulation

Individual data set results for the analysis in discussion section D for BMI-IM.

Q (nL/s)	$\langle v \rangle$	v_{unc}	$\langle \Phi \rangle$	Φ_{unc}
0.63	457.3	24.8	485.2	41.0
0.79	428.6	26.1	466.0	36.3
0.96	415.9	26.7	449.8	34.7
0.96	410.1	27.6	416.5	34.8
1.13	382.7	29.9	426.6	28.4
1.29	364.2	27.3	407.6	31.8
1.29	368.0	28.4	375.0	34.5
1.46	354.4	26.9	398.8	31.1
1.88	349.5	29.8	362.4	32.5

2.13	346.4	27.1	337.0	35.6
2.29	345.4	25.6	321.6	35.6
2.46	339.9	28.5	309.9	30.4

TABLE S1. Outputs of the best fits to the 12 individual BMI-IM data sets designed to best reproduce the centroid and FWHM values of the *high m/q* droplet distribution. The velocity values are units of m/s and the potential values are units of V. See figure 11.

S.3. *Physical Properties Reference Materials*

The determination of the physical properties of the ILs was achieved by averaging the values from 2-5 reference sources. The specific values from the available literature are for environmental conditions of temperatures at ~ 293 K and standard pressure of ~ 101 kPa. The dielectric values are for temperatures of ~ 298 K. The references for the average values for each IL are as follows: BMI-DCA – (Almeida *et al.* 2016; Carvalho *et al.* 2010; Engelmann *et al.* 2012; Kakinuma *et al.* 2017; Klomfar *et al.* 2011; Kong *et al.* 2014; Neves *et al.* 2013; Nieto de Castro *et al.* 2010; Sánchez *et al.* 2009; Stoppa *et al.* 2008; Zec *et al.* 2016; Zech *et al.* 2010), BMI-IM – (Alcalde *et al.* 2018; Almeida *et al.* 2016; Carvalho *et al.* 2008; Freire *et al.* 2007; Geppert-Rybczyńska *et al.* 2013; Klomfar *et al.* 2010; Li *et al.* 2019; Liu *et al.* 2018; Nieto de Castro *et al.* 2010; Ramenskaya *et al.* 2018; Salgado *et al.* 2014; Soldatović *et al.* 2017; Tokuda *et al.* 2005; Vraneš *et al.* 2014a; Vraneš *et al.* 2014b; Weingärtner 2006), BMI-BF₄ – (Almeida *et al.* 2016; Chaudhary *et al.* 2014; Ciocirlan *et al.* 2011; Fu *et al.* 2014; Gao & Wagner 2016; Grishina *et al.* 2013; Harris *et al.* 2008; Iglesias-Otero *et al.* 2007; Klomfar *et al.* 2010; Li *et al.* 2019; Matkowska & Hofman 2012; Pandit *et al.* 2016; Salgado *et al.* 2014; Sánchez *et al.* 2009; Sanmamed *et al.* 2010; Singh & Kumar 2008; Song & Chen 2014; Tokuda *et al.* 2006), and EMI-IM – (Annat *et al.* 2012; Bruce *et al.* 2017; Carvalho *et al.* 2008; Fillion *et al.* 2017; Geppert-Rybczyńska *et al.* 2010; Geppert-Rybczyńska *et al.* 2011; Hofmann *et al.* 2016; Jacquemin *et al.* 2007; Klomfar *et al.* 2010; Liu *et al.* 2018; Makino *et al.* 2014; Miran Beigi *et al.* 2013; Papović *et al.* 2016a; Papović *et al.* 2016b; Součková *et al.* 2012; Tariq *et al.* 2011; Tokuda *et al.* 2005; Weingärtner 2006).